energies

MDPI

Article

Heat Transfer Characteristics of Fractionalized Hydromagnetic Fluid with Chemical Reaction in Permeable Media

Basma Souayeh [1,2,*], Kashif Ali Abro [3,4], Nisrin Alnaim [1], Muneerah Al Nuwairan [5], Najib Hdhiri [2] and Essam Yasin [6]

1 Department of Physics, College of Science, King Faisal University, P.O. Box 400, Al-Ahsa 31982, Saudi Arabia; nalnaim@kfu.edu.sa
2 Laboratory of Fluid Mechanics, Physics Department, Faculty of Science of Tunis, University of Tunis EI Manar, Tunis 2092, Tunisia; hdhiri_najib@yahoo.fr
3 Faculty of Natural and Agricultural Sciences, Institute of Ground Water Studies, University of the Free State, Bloemfontein 9300, South Africa; kashif.abro@faculty.muet.edu.pk
4 Department of Basic Sciences and Related Studies, Mehran University of Engineering and Technology, Jamshoro 67480, Pakistan
5 Department of Mathematics and Statistics, College of Science, King Faisal University, P.O. Box 400, Al-Ahsa 31982, Saudi Arabia; msalnuwairan@kfu.edu.sa
6 Department of Mathematics, Statistics and Physics, College of Arts and Sciences, Qatar University, Doha P.O. Box 2713, Qatar; essamyasin@qu.edu.qa
* Correspondence: bsouayeh@kfu.edu.sa or basma.souayeh@gmail.com

Abstract: This manuscript optimizes the conjugate heat transfer and thermal-stress analysis for hydromagnetic Brinkman fluid with chemical reaction in permeable media. The governing equations of non-Newtonian Brinkman fluid have been traced out and then fractional derivative approach, namely, Caputo–Fabrizio, is invoked, subject to the exponential boundary conditions. The Fourier Sine and Laplace transforms are applied on governing partial differential equations for generating the analytical results of temperature, concentration and velocity. A comparative study of velocity field is investigated for the sake of long memory and hereditary properties. The analytical investigation of temperature, concentration and velocity field have strong effects on chemical reaction. The graphical depiction of vibrant characteristics of hydromagnetic Brinkman fluid with chemical reaction in permeable media is exhibited for disclosing the sensitivities of different embedded rheological parameters of fluid flow. The results suggested that temperature distribution for smaller and larger Prandtl number has disclosed quick and thicker heat diffusivity.

Keywords: fractional analysis; hydro-magnetized Brinkman fluid; Fourier analysis; permeable media

Citation: Souayeh, B.; Ali Abro, K.; Alnaim, N.; Al Nuwairan, M.; Hdhiri, N.; Yasin, E. Heat Transfer Characteristics of Fractionalized Hydromagnetic Fluid with Chemical Reaction in Permeable Media. *Energies* **2022**, *15*, 2196. https://doi.org/10.3390/en15062196

Academic Editor: Dmitry Eskin

Received: 15 February 2022
Accepted: 15 March 2022
Published: 17 March 2022

1. Introduction

Thermal stability usually refers to the deformed ability of an object under the influence of temperature with heat resistance of the material. Due to this reason, the prediction of thermal behavior among various fluids is essential for operating precision of heat and mass transfer. Particularly, the characteristics of fluids depend on their thermal performances because most of the researchers have diverted their mind to consider the convection effects; such effects occur in the Brinkman fluid flow, for which one needs to control the accuracy, stability, and efficiency of computational process for heterogeneous media [1–6]. Jiang et al. [7] investigated thermal conductivity characteristics based on carbon nanotubes experimentally, in which the Hamilton–Crosser model, Yu–Choi model and Xue model, so-called existent models for predicting thermal conductivity, were verified with help of the experiment. Their main purpose was to compare the thermal conductivity generated by nanofluids through the Yu–Choi model within different deviations. Chang et al. [8] analyzed the thermal analysis of Walters-B liquid model in a viscoelastic fluid from a vertical porous plate in which the numerical treatment was presented to the governing partial

differential equations with temperature and concentration distributions. They concluded that an increase in Schmidt number is observed to significantly decrease velocity profile as well as mass concentration. The boundary-layer flow and heat transfer characteristics in a second-grade fluid has been characterized by Rashid et al. [9] via modified differential transform method for analytical solutions. By taking the boundary conditions at infinity, the comparison between the solutions investigated via the differential transform method and the differential transform method Padé were presented on the basis of shooting method. Qasim et al. [10] investigated the thermal behavior of ferrofluid magnetohydrodynamic stretching cylinder in which thermal analysis on the basis of temperature and velocity has been justified by suspending the magnetic (Fe_3O_4) and non-magnetic (Al_2O_3) nanoparticles in base fluid. They concluded that the heat transfer rate and surface shear stress increase as the curvature parameter increases, which is why curvature helps to enhance the heat transfer. Gul et al. [11] investigated heat transfer on the basis of nanoparticles of magnetite, non-magnetic and aluminum oxide suspended in water as a base fluid. They considered mixed convection flow of ferrofluid along a vertical channel with physical boundary conditions. In order to achieve an appropriate thermal conductivity, they limited their study for magnetohydrodynamic fluid motion due to buoyancy force and applied pressure gradient. Ellahi et al. [12] modeled the nonlinear partial differential equations analytically for natural convection boundary layer flow for the enhancement heat transfer at a thermally moved vertical cone. Thermal conditions have been checked for the flow behavior on physical parameters Prandtl number and nanoparticle's volume fraction. Recently Ambreen et al. [13] suggested that how heat flow changes versus temperature on the rheology of magnetohydrodynamic fluid for the oscillations of heated plate. These authors used the Caputo–Fabrizio fractional operator for time on fluid model for the enhancement of thermal conductivities in which they concluded that higher Prandtl number leads to decay thermal diffusivity, which results in the reduction in thermal field. The thermal effects of magnetohydrodynamic micropolar fluid have been observed by Kashif et al. [14] with the Caputo–Fabrizio fractional derivative through Fourier analysis. They showed new results from hidden phenomenon of heat transfer for velocity field, mass concentration, microrotation and temperature distribution at some embedded parameters. The study on thermal analysis can be sustained, but we enlist here a few recent attempts therein [15–25] and for thermal analysis through fractional techniques are [26–31]. Additionally, some recent work is embedded in [32–38] based on different approaches for the enhancement of heat transfer. Motivated by the above discussions, our aim is to explore the optimized and conjugate heat transfer and thermal-stress analysis for hydromagnetic Brinkman fluid with chemical reaction in permeable media. The governing equations of non-Newtonian Brinkman fluid have been traced out and then a fractional derivative approach, namely, Caputo–Fabrizio, has been functionalized subject to exponential boundary conditions. The Fourier analysis and Laplace transform techniques are implemented on governing partial differential equations for generating the analytical results of temperature, concentration, and velocity. A comparative study based on mathematical expressions of velocity field is investigated for the description of long memory and hereditary properties from fractionalized analytical solutions. The graphical depiction for vibrant characteristics of hydromagnetic Brinkman fluid with chemical reaction in permeable media is exhibited for disclosing the sensitivities of different embedded rheological parameters of fluid flow.

2. Mathematical Model for Free Convection Problem of Brinkman Fluid

Consider an electrically conducting flow of the unsteady free convectional Brinkman fluid embedded in porous medium within an incompressibility condition. The exponentially heated plate is taken in the xz-plane of a Cartesian coordinate system. Here, the x-axis is set in vertical direction and y-axis is normal to it. Initially, the fluid and plate both are taken stationary at $t = 0$. The fluid above the heated plate begins to move when $t = 0^+$ due to the exponential shear stress. The governing boundary layer equations are taken

into account by using the Boussinesq's approximation along with sketched geometry in Figure 1.

$$\begin{aligned}
&\frac{\partial w(y,t)}{\partial t} + \left(\beta_1 + \frac{\mu O}{K} + \frac{B_0^2\sigma}{\rho}\right) w(y,t) = v\frac{\partial^2 w(y,t)}{\partial y^2} + g\beta_T(T(y,t) - T_\infty) + g\beta_C(C(y,t) - C_\infty); y > 0,\\
&\frac{\partial T(y,t)}{\partial t} = \frac{k}{\rho C_p}\frac{\partial^2 T(y,t)}{\partial y^2}; y > 0,\\
&\frac{\partial C(y,t)}{\partial t} = D\frac{\partial^2 C(y,t)}{\partial y^2} - \theta(C(y,t) - C_\infty); y > 0.
\end{aligned} \tag{1}$$

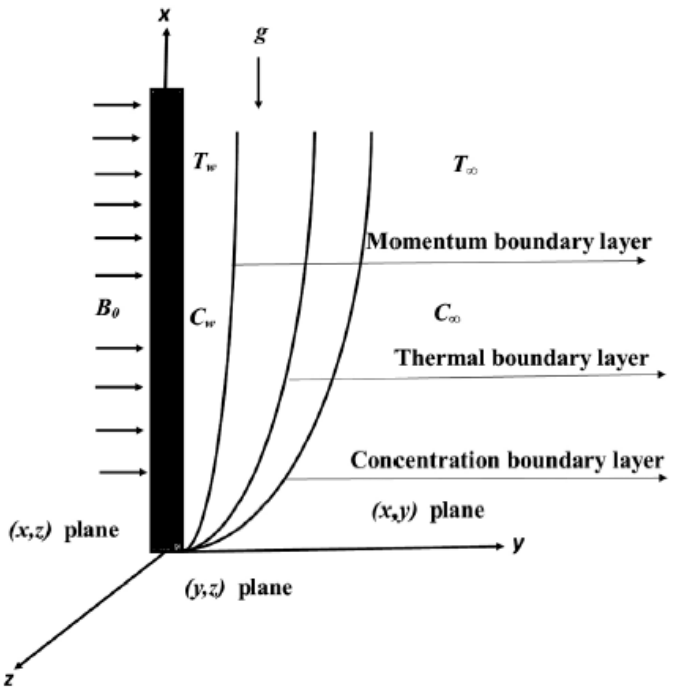

Figure 1. Physical geometry.

Equation (1) is subjected to following initial and boundary conditions as:

$$\begin{aligned}
&w(y,0) = 0, T(y,0) = T_\infty, C(y,0) = C_\infty,\\
&w(0,t) = \Re e^{at},\ T(0,t) = T_w,\ C(0,t) = C_\infty\\
&w(\infty,t) = 0, T(\infty,t) = T_\infty, C(\infty,t) = C_\infty.
\end{aligned} \tag{2}$$

Here, the fluid's velocity, temperature and concentration are symbolized as $w(y,t)$, $T(y,t)$ and $C(y,t)$, respectively. Different rheological parameters are typically set, such as β_1 is the Brinkman type fluid, ν as the kinematic viscosity, g is the gravitational acceleration, μ is the dynamic viscosity, β_T is the coefficient of thermal expansion, β_C is the coefficient of mass expansion, ρ is the density of the fluid, C_p is the specific heat at constant pressure, D is the mass diffusivity, θ is the chemical reaction, k is the coefficient of mass diffusion, ϕ is the permeability of the porous medium, K is the porosity, B_0^2 is the applied magnetic field's magnitude, and σ is the electrical conductivity of the fluid. In this connection, implementing the non-integer order derivative Caputo–Fabrizio as defined in Equation (3):

$$\frac{\partial^\delta w(y,t)}{\partial t^\delta} = \frac{1}{1-\delta}\int_0^t \exp\left(\frac{-\delta(z-t)}{1-\delta}\right) w'(y,t)dt, \qquad 0 \le \delta \le 1. \tag{3}$$

Additionally, invoking the non-dimensional quantities as described

$$\begin{gathered} w^* = w\Re^{-1}, y^* = \Re y v^{-1}, t^* = tv^{-1}, \Phi = \nu\mu\phi\left(\Re_0^3\rho k\right)^{-1}, M = vB_0^2\sigma\left(\Re_0^3\rho\right)^{-1}, Pr = \mu C_p k^{-1}, \\ Sc = vD^{-1}\theta = D^{-1}k\gamma^2, Gm = \Re^{-2}g\beta_C(C_\omega - C_\infty), G_r = \Re^{-2}g\beta_T(T_\omega - T_\infty), \\ T^* = (T - T_\infty)(T_w - T_\infty)^{-1}, C^* = (C - C_\infty)(C_w - C_\infty)^{-1}. \end{gathered} \tag{4}$$

Substituting Equations (3) and (4) into Equations (1) and (2), we transferred the governing equations for the momentum, energy and concentration as written below:

$$\frac{\partial^\delta w(y,t)}{\partial t^\delta} + (M + \beta_1 + \Phi)w(y,t) = \nu\frac{\partial^2 w(y,t)}{\partial y^2} + Gm\, C(y,t) + Gr\, T(y,t), \tag{5}$$

$$Pr\frac{\partial^\delta T(y,t)}{\partial t^\delta} = \frac{\partial^2 T(y,t)}{\partial y^2}, \tag{6}$$

$$Sc\frac{\partial^\delta C(y,t)}{\partial t^\delta} = \frac{\partial^2 C(y,t)}{\partial y^2} - \theta C(y,t). \tag{7}$$

Here, Gm is the mass Grashof number, Gr is the thermal Grashof number, Pr is the Prandtl number, Sc is the Schmidt number and θ is the coefficient of mass diffusion. The imposed conditions are

$$\begin{gathered} w(0,t) = \Re e^{at},\ T(0,t) = t, C(0,t) = t\ ,\ t > 0, \\ w(y,0) = 0,\ T(y,0) = 0,\ C(y,0) = 0\ ,\ y > 0, \\ w(y,t) \to 0,\ T(y,t) \to 0,\ C(y,t) \to 0,\ y \to \infty,\ t > 0. \end{gathered} \tag{8}$$

Manipulation of accurate solution is necessary for physical interpretation from the set of governing Equations (5)–(8). Initially, Equations (5)–(7) are modeled by non-integer order derivative Caputo–Fabrizio. We can intricate coupled differential Equations (5)–(7) by means of Fourier and Laplace transform methods.

3. Integral Transforms Approach for the Solution of Problem

3.1. Solution of Temperature

Applying the Fourier sine transform on spatial variable involved in linearized and fractionalized differential Equations (5) and (8), we have

$$\left(\sqrt{\frac{2}{\pi}}\frac{\xi}{Pr}\right)^{-1}\left(\frac{\partial^\delta}{\partial t^\delta} + \frac{\xi^2}{Pr}\right)T_s(\xi,t) = T_s(0,t), \tag{9}$$

where an image of Fourier sine transform of $T(y,t)$ is $T_s(\xi,t)$ has to validate the imposed conditions (8). We combine Fourier sine transform method with the Laplace transform method for the solution of fractional derivative involved in Equation (9); we apply the Laplace Transform on Equation (9) as

$$\sqrt{\pi}\left(q^2\left(\xi^2 + \tau_0 Pr\right)(q + \tau_2)\right)\overline{T_s}(\xi,q) = \sqrt{2}\xi(q + \tau_1), \tag{10}$$

We introduce the rheological parameters involved in Equation (10) as $\tau_0 = \frac{1}{1-\delta}$, $\tau_1 = \tau_0\delta$, $\tau_2 = \frac{\tau_1\xi^2}{(\xi^2 + Pr\ \tau_0)}$. Writing Equation (10) into equivalent form then applying Fourier sine transform, we get

$$\overline{T}(y,q) = \frac{2}{\pi}\int_0^\infty \sin(y\xi)\left\{\xi^{-1}q^{-2} - \frac{(q + \tau_2)^{-1}Pr\tau_0\xi^{-1}}{(Pr\ \tau_0 + \xi^2)q}\right\}d\xi, \tag{11}$$

Pertaining to the processes of integral $\int_0^\infty \frac{\sin(y\xi)}{\xi} d\xi = \frac{\pi}{2}$ on Equation (11) and inverting by means of Laplace transform, the final solution of temperature distribution is

$$T(y,t) = t - \frac{4Pr\tau_0\xi^{-1}\pi^{-2}}{(\sqrt{\tau_2}\xi^2 + \sqrt{\tau_2}Pr\ \tau_0)} \int_0^\infty \int_0^{\sqrt{\tau_2 t}} t^{1/2} e^{\tau^2 - \tau_2 t} \sin(y\xi)\ d\xi d\tau. \tag{12}$$

Equation (12) can be verified for imposed initial and boundary conditions as discussed in Equation (8).

3.2. Solution of Concentration

Applying the Fourier sine transform on spatial variable involved in linearized and fractionalized differential Equations (6) and (8), we have

$$\left(\sqrt{\frac{2}{\pi}}\frac{\xi}{Sc}\right)^{-1}\left(\frac{\partial^\delta}{\partial t^\delta} + \frac{\xi^2}{Sc}\right)C_s(\xi,t) = C_s(0,t), \tag{13}$$

where an image of Fourier sine transform of $C(y,t)$ is $C_s(\xi,t)$ has to validate the imposed conditions (8). We combine Fourier sine transform method with the Laplace transform method for the solution of fractional derivative involved in Equation (13); we apply the Laplace Transform on Equation (13) as

$$\sqrt{\pi}\Big(q^2\Big(\xi^2 + \tau_0 Sc + \theta\Big)(q + \tau_5)\Big)\overline{C_s}(\xi,q) = \sqrt{2}\xi(q + \tau_1), \tag{14}$$

We introduce the rheological parameters involved in Equation (14) as $\tau_3 = \frac{\tau_1\xi^2}{(\xi^2 + Sc\ \tau_0)}$, $\tau_4 = \tau_1\left(\xi^2 + \theta\right)$ and $\tau_5 = \frac{\tau_3}{\tau_4}$. Writing Equation (14) into equivalent form then applying Fourier sine transform, we get

$$\overline{C}(y,q) = \frac{2}{\pi}\int_0^\infty \sin(y\xi)\left\{\xi^{-1}q^{-2} - \frac{(q+\tau_5)^{-1}Sc\tau_0\xi^{-1}}{(Sc\ \tau_0 + \xi^2 + \theta)q}\right\}d\xi, \tag{15}$$

Pertaining to the processes of integral $\int_0^\infty \frac{\sin(y\xi)}{\xi} d\xi = \frac{\pi}{2}$ on Equation (15) and inverting by means of Laplace transform, we finalize solution of temperature distribution as

$$C(y,t) = t - \frac{4Sc\tau_0\xi^{-1}\pi^{-2}}{(\theta\sqrt{\tau_5} + \sqrt{\tau_5}\xi^2 + \sqrt{\tau_5}Sc\tau_0)} \int_0^\infty \int_0^{\sqrt{\tau_5 t}} t^{1/2} e^{\tau^2 - \tau_5 t} \sin(y\xi)\ d\xi d\tau. \tag{16}$$

Equation (16) can be verified for imposed initial and boundary conditions as discussed in Equation (8).

3.3. Solution of Velocity

Applying the Fourier sine transform on the spatial variable involved in linearized and fractionalized differential Equations (7) and (8), we have

$$\left(\sqrt{\frac{2}{\pi}}v\xi\right)^{-1}\left\{\frac{\partial\delta}{\partial t^\delta} + \Big(M + v\xi^2 + \beta_1 + \Phi\Big)\right\}w_s(\xi,t) - G_m C_s(\xi,t) - G_r T_s(\xi,t) = w_s(0,t) \tag{17}$$

where an image of Fourier sine transform of $w(y,t)$ is $w_s(\xi,t)$ has to validate the imposed conditions (8). We combine Fourier sine transform method with the Laplace transform

method for the solution of fractional derivative involved in Equation (17); we apply the Laplace Transform on Equation (17) as

$$w_s(\xi,q)=\sqrt{\frac{2}{\pi}}\,\xi\left[\left\{\left(\Re M+\Re\nu\xi^2+\Re\beta_1+\Re\Phi\right)+q\tau_0\left(\frac{q-a}{q+\tau_1}\right)\right\}^{-1}+\frac{(q+\tau_1)^2}{q^2(q\tau_6+\tau_7)}\right.$$
$$\left.\times\frac{Gr}{(q(P_r\tau_0+\xi^2)+\xi^2\tau_1)}+\frac{Gm}{(q(S_c\tau_0+\xi^2+\theta)+\xi^2\tau_1+\theta\tau_1)}\right], \tag{18}$$

We introduce the rheological parameters involved in Equation (18) as $\tau_6=\Phi+\tau_0+\xi^2+M+\beta_1$ and $\tau_7=\Phi\tau_1+\xi^2\tau_1+\beta_1\tau_1+M\tau_1$. Writing Equation (18) into equivalent form then applying Fourier sine transform, we get

$$\overline{w}(y,q)=\Re(q-a)^{-1}-\frac{2\xi^{-1}(\tau_6+\xi^2)\Re}{\pi\tau_6}\int_0^\infty\sin(y\xi)\frac{(q+\tau_8)}{(q+\tau_9)(q-a)}d\xi+\frac{2Gr\xi^{-1}}{\pi(\tau_6P_r\tau_0+\xi^2\tau_6)}\int_0^\infty\sin(y\xi)$$
$$\times\frac{(q+\tau_1)^2}{q^2(q+\tau_2)(q+\tau_9)}d\xi+\frac{2Gm\xi^{-1}}{\pi(\tau_6S_c+\tau_6\xi^2+\tau_6\theta)}\int_0^\infty\sin(y\xi)\frac{(q+\tau_1)^2}{q^2(q+\tau_5)(q+\tau_9)}d\xi, \tag{19}$$

Here, $\tau_8=\frac{\tau_7+\xi^2\tau_1}{\tau_7+\xi^2}$ and $\tau_9=\frac{\tau_7}{\tau_6}$ are letting parameters for the simplification. Pertaining to the processes of integral $\int_0^\infty\frac{\sin(y\xi)}{\xi}d\xi=\frac{\pi}{2}$ on Equation (19) and inverting by means of Laplace transform, we finalize solution of temperature distribution as

$$w(y,t)=\Re e^{at}-\frac{2\xi^{-1}(\tau_6+\xi^2)\Re}{\pi\tau_6(\tau_8-\tau_9)^{-1}}\int_0^\infty\int_0^t\sin(y\xi)e^{(a-\tau_9)t-a\tau}d\tau\,d\xi+\frac{2\xi^{-1}Gr}{(\pi\tau_6P_r\tau_0+\pi\tau_6\xi^2)}\int_0^\infty\sin(y\xi)$$
$$\times\left\{\frac{2\tau_1+\tau_1^2t}{\tau_2\tau_9}-\frac{\tau_1^2(\tau_2+\tau_9)}{(\tau_2\tau_9)^2}+\frac{e^{-\tau_2t}}{(\tau_9-\tau_2)}-\frac{2\tau_1e^{-\tau_2t}}{\tau_2(\tau_9-\tau_2)}+\frac{\tau_1^2e^{-\tau_2t}}{\tau_2^2(\tau_9-\tau_2)}+\frac{e^{-\tau_9t}}{(\tau_2-\tau_9)}-\frac{2\tau_1e^{-\tau_9t}}{\tau_9(\tau_2-\tau_9)}\right.$$
$$\left.+\frac{\tau_1^2e^{-\tau_9t}}{\tau_9^2(\tau_2-\tau_9)}\right\}d\xi+\frac{2\xi^{-1}Gm}{(\pi\tau_6S_c\tau_0+\pi\tau_6\xi^2+\pi\tau_6\theta)}\int_0^\infty\sin(y\xi)\left\{\frac{2\tau_1+\tau_1^2t}{\tau_5\tau_9}-\frac{\tau_1^2(\tau_5+\tau_9)}{(\tau_5\tau_9)^2}+\frac{e^{-\tau_5t}}{(\tau_9-\tau_5)}\right.$$
$$\left.-\frac{2\tau_1e^{-\tau_5t}}{\tau_5(\tau_9-\tau_5)}+\frac{\tau_1^2e^{-\tau_5t}}{\tau_5^2(\tau_9-\tau_5)}+\frac{e^{-\tau_9t}}{(\tau_5-\tau_9)}-\frac{2\tau_1e^{-\tau_9t}}{\tau_9(\tau_5-\tau_9)}+\frac{\tau_1^2e^{-\tau_9t}}{\tau_9^2(\tau_5-\tau_9)}\right\}d\xi. \tag{20}$$

We utilized the following Equations (21) and (22) for inverting Equation (19) by means of Laplace transform to have Equation (20) as

$$\mathcal{L}^{-1}\left\{\frac{s+b}{s+c}\right\}=(b-c)exp(-ct), \tag{21}$$

$$\mathcal{L}^{-1}\left\{\frac{s^2+a_1s+a_0}{s^2(s+a)(s+b)}\right\}=\frac{a_1+a_0t}{ab}-\frac{a_0(a+b)}{(ab)^2}+\frac{e^{-at}}{b-a}+\frac{e^{-bt}}{a-b}-\frac{a_1e^{-at}}{a(b-a)}-\frac{a_1e^{-bt}}{b(a-b)}+\frac{a_0e^{-at}}{a^2(b-a)}+\frac{a_0e^{-bt}}{b^2(a-b)}. \tag{22}$$

Equation (20) can be verified for imposed initial and boundary conditions as discussed in Equation (8).

3.4. Particular Solutions of Concentration and Velocity without Chemical Reaction

The general solutions in the absence of chemical reaction have importance in the chemical engineering for mixing the chemical reactions or ecology, such fields arise in physics. The general solutions of concentration and velocity can be investigated in the absence of chemical reaction by substituting $\theta=0$ in Equations (16) and (20). For the sake of general solutions of concentration and velocity in the absence of chemical reaction, we obtain

$$C(y,t)=t-\frac{4Sc\tau_0\xi^{-1}\pi^{-2}}{(\sqrt{\tau_{11}}\xi^2+\sqrt{\tau_{11}}Sc\tau_0)}\int_0^\infty\int_0^{\sqrt{\tau_{11}t}}t^{1/2}e^{\tau^2-\tau_{11}t}\sin(y\xi)\,d\xi d\tau. \tag{23}$$

$$w(y,t) = \Re e^{at} - \frac{2\xi^{-1}(\tau_6+\xi^2)\Re}{\pi\tau_6(\tau_8-\tau_9)^{-1}} \int_0^\infty \int_0^t \sin(y\xi) e^{(a-\tau_9)t-a\tau} d\tau\, d\xi + \frac{2\xi^{-1}Gr}{(\pi\tau_6 P_r\tau_0+\pi\tau_6\xi^2)} \int_0^\infty \sin(y\xi)$$
$$\times \left\{ \frac{2\tau_1+\tau_1^2 t}{\tau_2\tau_9} - \frac{\tau_1^2(\tau_2+\tau_9)}{(\tau_2\tau_9)^2} + \frac{e^{-\tau_2 t}}{(\tau_9-\tau_2)} - \frac{2\tau_1 e^{-\tau_2 t}}{\tau_2(\tau_9-\tau_2)} + \frac{\tau_1^2 e^{-\tau_2 t}}{\tau_2^2(\tau_9-\tau_2)} + \frac{e^{-\tau_9 t}}{(\tau_2-\tau_9)} - \frac{2\tau_1 e^{-\tau_9 t}}{\tau_9(\tau_2-\tau_9)} \right.$$
$$\left. + \frac{\tau_1^2 e^{-\tau_9 t}}{\tau_9^2(\tau_2-\tau_9)} \right\} d\xi + \frac{2\xi^{-1}Gm}{(\pi\tau_6 S_c\tau_0+\pi\tau_6\xi^2)} \int_0^\infty \sin(y\xi) \left\{ \frac{2\tau_1+\tau_1^2 t}{\tau_{11}\tau_9} - \frac{\tau_1^2(\tau_{11}+\tau_9)}{(\tau_{11}\tau_9)^2} + \frac{e^{-\tau_{11} t}}{(\tau_9-\tau_{11})} \right.$$
$$\left. - \frac{2\tau_1 e^{-\tau_{11} t}}{\tau_{11}(\tau_9-\tau_{11})} + \frac{\tau_1^2 e^{-\tau_{11} t}}{\tau_{11}^2(\tau_9-\tau_{11})} + \frac{e^{-\tau_9 t}}{(\tau_{11}-\tau_9)} - \frac{2\tau_1 e^{-\tau_9 t}}{\tau_9(\tau_{11}-\tau_9)} + \frac{\tau_1^2 e^{-\tau_9 t}}{\tau_9^2(\tau_{11}-\tau_9)} \right\} d\xi. \quad (24)$$

Equations (22) and (23) have been investigated with help of letting parameters as $\tau_{10} = \tau_1\xi^2$ and $\tau_{11} = \frac{\tau_3}{\tau_{10}}$. Meanwhile, Equations (23) and (24) can be verified for imposed initial and boundary conditions as discussed in Equation (8). Furthermore, one can also investigate the solutions in the absence of magnetic field and preamble media by letting $M = \Phi = 0$ from Equation (20).

3.5. Expressions of Nusselt and Sherwood Numbers and Skin Friction

The role of Nusselt number is to give the ratio of thermal energy convected to the thermal energy conducted within the fluid. The expression of Nusselt number can be obtained by Nusselt number $= \mathrm{Nu} = \mathcal{L}^{-1}\left(\lim_{y\to 0}\frac{\partial T(y,q)}{\partial y}\right) = \left.\frac{\partial T(y,t)}{\partial y}\right|_{y=0}$. The Role of Sherwood number is to provide the ratio of the convective mass transfer to the rate of diffusive mass transport. The expression of Sherwood number can be obtained by Sherwood number $= \mathrm{Sh} = \mathcal{L}^{-1}\left(\lim_{y\to 0}\frac{\partial C(y,q)}{\partial y}\right) = \left.\frac{\partial C(y,t)}{\partial y}\right|_{y=0}$. The Role of Skin friction is to observe the resistance to the laminar flow of an object moving through a fluid. The expression of Skin friction can be obtained by $Skin\ friction = C_f = \mathcal{L}^{-1}\left(\lim_{y\to 0}\frac{\partial w(y,q)}{\partial y}\right) = \left.\frac{\partial w(y,t)}{\partial y}\right|_{y=0}$.

4. Parametric Results

In summary, an optimization of fractional model of hydromagnetic Brinkman fluid with a chemical reaction in permeable media is proposed, subject to an application of the non-Newtonian fluid. Fractional calculus is introduced to characterize the conjugate heat transfer and thermal-stress analysis. In addition, the superiority of the proposed model is tested via the Fourier analysis and Laplace transform techniques on temperature, concentration and velocity. A comparative study based on mathematical expressions of velocity field is investigated for the description of long memory and hereditary properties from fractionalized analytical solutions. The graphical depiction for vibrant characteristics of hydromagnetic Brinkman fluid with chemical reaction in permeable media is exhibited for disclosing the sensitivities of different embedded rheological parameters of fluid flow. On the basis of the above discussion, with a theoretical point of view, we depicted graphical illustrations in which interesting outcomes have been underlined and obtained. Figure 2 is depicted for the temperature distribution on the basis of a condition imposed on the Prandtl number in terms of 2D and 3D. The Prandtl number is considered smaller as $P_r = 0.1, 0.3, 0.5, 0.7$ for disclosing the hidden characteristics of the fluid. In order to achieve heat diffusivity quickly, we have observed the smaller as $P_r = 0.1, 0.3, 0.5, 0.7$ on temperature distribution. It is quite clear from Figure 2 that thermal boundary layer is much thicker, due to the consideration of smaller number. The shear component for diffusivity, viscosity and density to the diffusivity can be illustrated by means of proper choice of Schmidt number, such phenomenon is observed in Figure 3. Mass concentration is discussed by means of Schmidt number subject to investigating the relative thickness of the hydrodynamic layer and mass-transfer boundary layer. It is further noted that mass concentration has decreasing behavior as Schmidt number increases. The magnetic influences on fluid the motion is elucidated for velocity field in Figure 4 for pulling and attracting the magnetic particles from the fluids. It is quite clear from Figure 4 that the velocity field

is completely repelled due to magnetic effects applied on fluid. The behavior depicted in Figure 4 for velocity field shows that those intrinsic properties of the magnetic field cause a reduction in the fluid flow. From a physical point of view, the Hall effects (magnitude of a magnetic field) were measured on due to Lorentz forces. In order to describe the fraction of void space in the fluid, we presented Figure 5 for the effective role of porosity on the velocity field. The porosity has an interesting behavior on velocity field because the fluid type is Brinkman, such fluids already have the maximum amount of pour structures, and such a phenomenon is always proportional to hydraulic conductivity. In our case, increasing the values of porosity enhances the velocity field. It is also observed that role of the magnetic field and the porosity on the velocity field is reciprocal. A comparative analysis is performed for fractional verses non-fractional operators in Figures 6–8 for the behavior of velocity field and temperature distribution with and without magnetic field and porosity. Figure 6 is for a comparison of three types of models: (i) velocity with the CF approach with magnet, (ii) velocity with the CF approach without magnet, and (iii) velocity with non-fractional approach with magnet. It is clear from Figure 6 that velocity with the CF approach with magnet is higher than velocity with the CF approach without magnet and velocity with non-fractional approach with magnet. On the other hand, Figure 7 is prepared for the comparison of three types of models in which (i) a velocity with the CF approach with porous, (ii) a velocity with the CF approach without porous and (iii) a velocity with non-fractional approach with porous. Here, the similar trend is observed in comparison with magnetic field. The comparison of temperature distribution is also highlighted on the effective role of chemical reaction with fractional verses non-fractional techniques in Figure 8. We present here four models based on chemical reaction involved in temperature distribution: (i) temperature with the CF approach with chemical reaction, (ii) temperature with the CF approach without chemical reaction, (iii) temperature with classical approach with chemical reaction and (iv) temperature with classical approach without chemical reaction. Here, it is observed how new forms of temperature distribution are investigated reciprocally in comparison with Figures 6 and 7. Meanwhile, the temperature with the CF approach with chemical reaction has a lower velocity than the other three types of temperature distribution models. This may be due to the fact that the chemical reactions help in investigating the crucial role of temperature distribution to understand the properties of Brinkman fluid flow on the basis of a non-singular kernel involved in the Caputo–Fabrizio fractional operator.

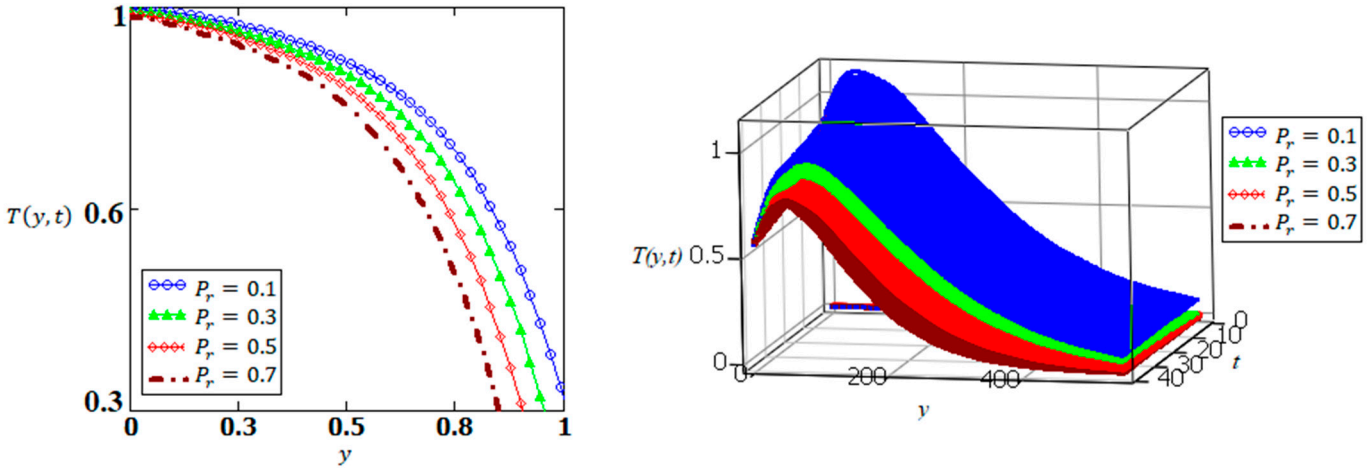

Figure 2. Effective role of temperature distribution depicted from Equation (12) for P_r.

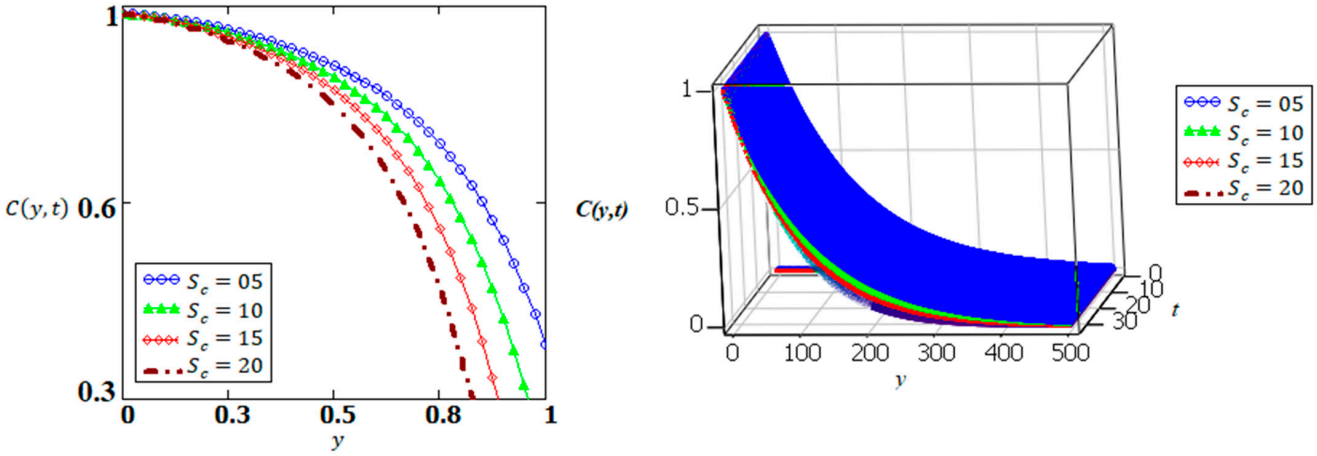

Figure 3. Effective role of mass concentration depicted from Equation (16) for S_c.

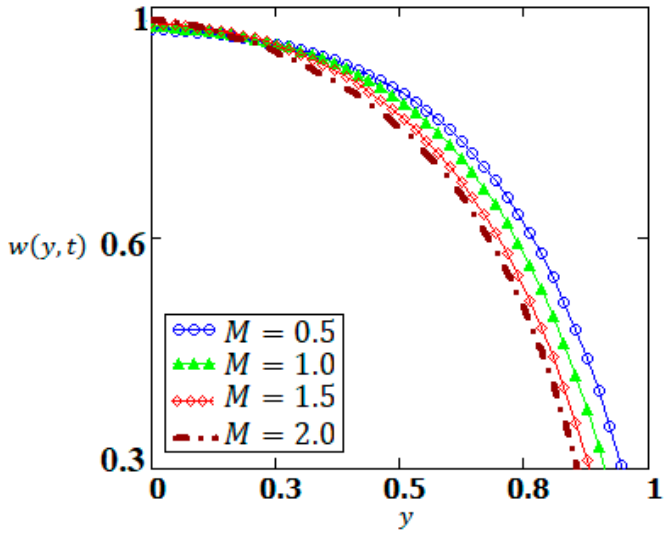

Figure 4. Effective role of velocity field depicted from Equation (19) for M.

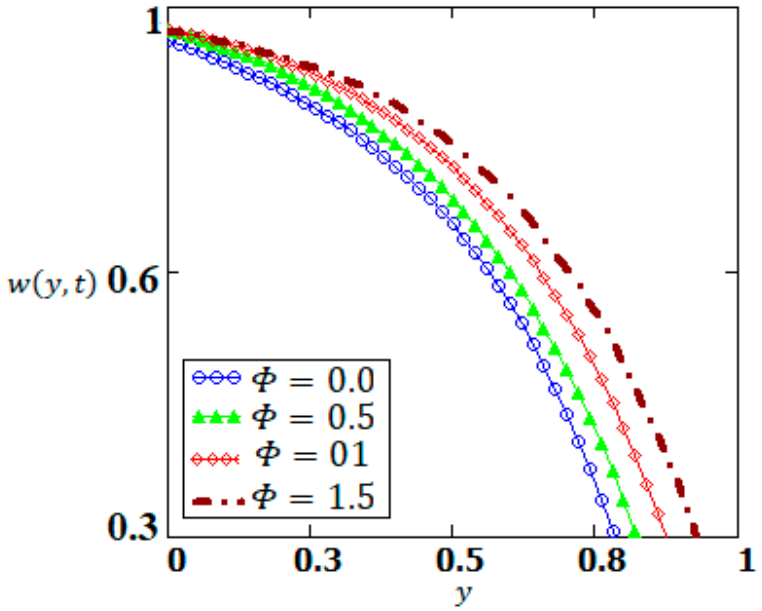

Figure 5. Effective role of velocity field depicted from Equation (19) for Φ.

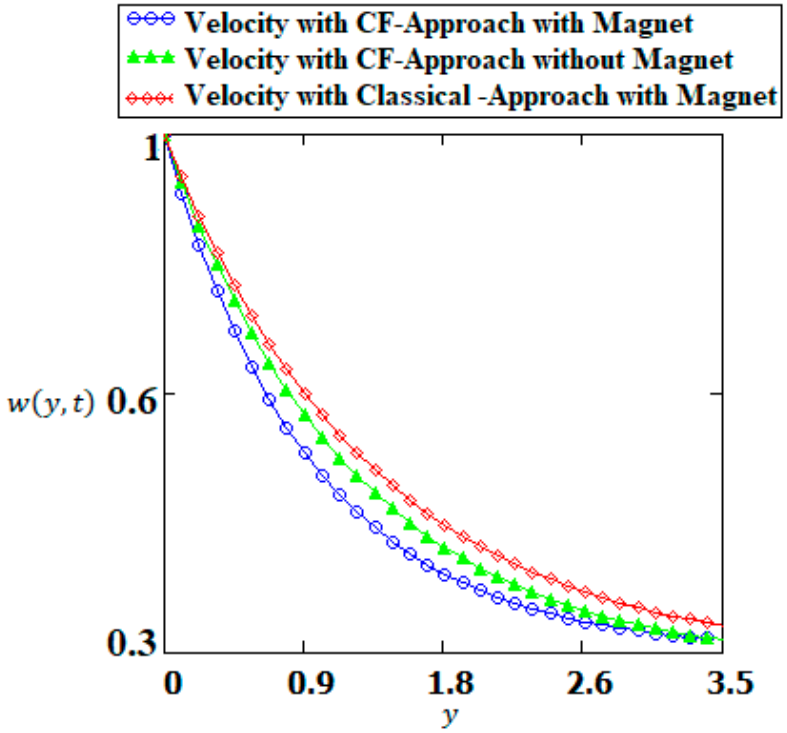

Figure 6. Comparison of velocity field depicted from Equation (19) with $M = 0$ and $\delta \neq 1$, Equation (19) for $M \neq 0$ and $\delta \neq 1$, Equation (19) for $M \neq= 0$ and $\delta = 1$.

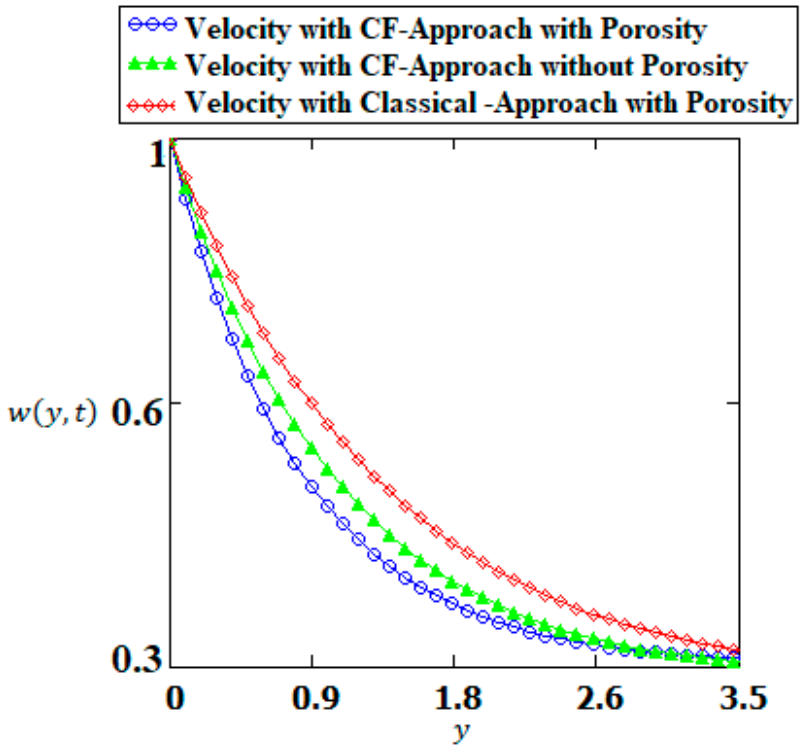

Figure 7. Comparison of velocity field depicted from Equation (19) with $\Phi = 0$ and $\delta \neq 1$, Equation (19) for $\Phi \neq 0$ and $\delta \neq 1$, Equation (19) for $\Phi \neq 0$ and $\delta = 1$.

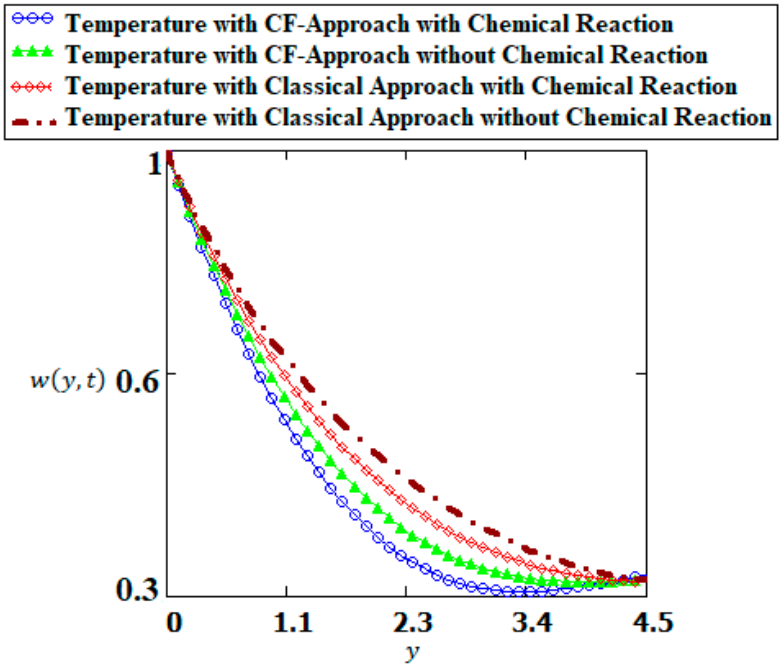

Figure 8. Comparison of velocity field depicted from Equation (11) with $\theta \neq 0$ and $\delta \neq 1$, Equation (11) for $\theta = 0$ and $\delta \neq 1$, Equation (11) for $\theta \neq 0$ and $\delta = 1$ and Equation (11) for $\theta = 0$ and $\delta = 1$.

5. Conclusions

The conjugate heat transfer and thermal-stress analysis for hydromagnetic Brinkman fluid with chemical reaction in permeable media is investigated. Non-Newtonian Brinkman fluid with exponential boundary conditions is analyzed with help of Fourier Sine and Laplace transforms. The analytical results of temperature, concentration and velocity have been established via long memory and hereditary properties. The characteristics of hydromagnetic Brinkman fluid with chemical reaction in permeable media has exhibited the following rheological outcomes:

- The temperature distribution for a smaller and larger Prandtl number has disclosed quick and thicker heat diffusivity;
- Mass concentration has a decreasing behavior as the Schmidt number increases; this is because of the relative thickness of the hydrodynamic layer;
- The repelled magnetic effects have been observed in the velocity field due to the intrinsic properties of the magnetic field causing a reduction in the fluid flow;
- Increasing values of porosity that enhances the velocity field;
- The velocity via the CF approach with magnet is faster than velocity via the CF approach without magnet;
- Temperature via the CF approach with chemical reaction has slower distribution. Physically, chemically reacting temperatures comprise with Arrhenius activation energy at different rates.

6. Future Directions

For the sake of an optimization of the fractional model of hydromagnetic Brinkman fluid with a chemical reaction in permeable media, the same mathematical model of magnetized Cassion fluid can be extended by the following:

- A comparative study of magnetized Cassion fluid can be investigated through fractal differential operator with fractional differential operator;
- The similar problem can be traced out for optimal heat transfer via Keller-Box method and Lie group theory;
- The magnetized Cassion fluid model can be modified for newly developed boundary conditions namely Mittag–Leffler function.

Author Contributions: Conceptualization, B.S. and K.A.A.; methodology, B.S. and K.A.A.; software, B.S. and K.A.A.; validation, N.A., B.S. and N.H.; formal analysis, E.Y.; investigation, K.A.A.; resources, B.S.; data curation, M.A.N.; writing—original draft preparation, N.H.; writing—review and editing, M.A.N. and N.A.; visualization, E.Y.; supervision, B.S.; project administration, K.A.A.; funding acquisition, B.S. All authors have read and agreed to the published version of the manuscript.

Funding: This work was supported by the Deanship of Scientific Research, Vice Presidency for Graduate Studies and Scientific Research, King Faisal University, Saudi Arabia [Project No. GRANT233].

Data Availability Statement: The data that support the findings of this study are available from the corresponding author upon reasonable request.

Acknowledgments: This work was supported by the Deanship of Scientific Research, Vice Presidency for Graduate Studies and Scientific Research, King Faisal University, Saudi Arabia [Project No. GRANT233].

Conflicts of Interest: The authors declare there is no conflict of interest for this submission.

Nomenclature

$w(y,t)$	Velocity field
$T(y,t)$	Temperature distribution
$C(y,t)$	Mass concentration
β_1	Brinkman type fluid parameter
ν	Kinematic viscosity
g	Gravitational acceleration
μ	Dynamic viscosity
β_T	Coefficient of thermal expansion
β_C	Coefficient of mass expansion
ρ	Density of the fluid
C_p	Specific heat at constant pressure
D	Mass diffusivity
θ	Chemical reaction
k	Coefficient of mass diffusion
ϕ	Permeability of the porous medium
K	Porosity
B_0^2	Magnitude applied magnetic field,
σ	Electrical conductivity of the fluid.
$\frac{\partial^\delta}{\partial t^\delta}$	Non-integer order derivative of Caputo–Fabrizio.
δ	Fractional differential parameter
Gm	Mass Grashof number
Gr	Thermal Grashof number
Pr	Prandtl number
S_C	Schmidt number
θ	Coefficient of mass diffusion
$\mathcal{R}$	Non-zero parameter
y	Spatial variable
t	Time variable
ξ	Fourier Sine transformed variable
$\tau_0 - \tau_{11}$	Letting parameters
M	Magnetic field
Φ	Preamble media

References

1. Hdhiri, N.; Ben-Beya, B.; Lili, T. Effects of internal heat generation or absorption on heat transfer and fluid flow within partially heated square enclosure: Homogeneous fluids and porous media. *J. Porous Media* **2015**, *18*, 415–435. [CrossRef]
2. Hdhiri, N.; Ben-Beya, B. Numerical study of laminar mixed convection flow in a lid-driven square cavity filled with porous media: Darcy -Brinkman-Forchheimer and Darcy-Brinkman models. *Int. J. Numer. Methods Heat Fluid Flow* **2018**, *28*, 857–877. [CrossRef]

3. Hu, X.Q.; Chen, W.F. Thermal characteristics analysis and experiment for angular contact ball bearing. *J Xi'an Jiaotong Univ.* **2015**, *49*, 106–110.
4. Kashif, A.A.; Ilyas, K. Analysis of Heat and Mass Transfer in MHD Flow of Generalized Casson Fluid in a Porous Space Via Non-Integer Order Derivative without Singular Kernel. *Chin. J. Phys.* **2017**, *55*, 1583–1595.
5. Arshad, K.; Kashif, A.A.; Asifa, T.; Ilyas, K. Atangana-Baleanu and Caputo Fabrizio Analysis of Fractional Derivatives for Heat and Mass Transfer of Second Grade Fluids over a Vertical Plate: A Comparative study. *Entropy* **2017**, *19*, 279.
6. Abro, K.A.; Mukarrum, H.; Mirza, M.B. An Analytic Study of Molybdenum Disulfide Nanofluids Using Modern Approach of Atangana-Baleanu Fractional Derivatives. *Eur. Phys. J. Plus* **2017**, *132*, 439. [CrossRef]
7. Jiang, W.; Ding, G.; Pang, H. Measurement and model on thermal conductivities of carbon nanotube nanorefrigerants. *Int. J. Therm. Sci.* **2009**, *48*, 1108–1115. [CrossRef]
8. Chang, T.B.; Mehmood, A.; Beg, O.A.; MNarahari, M.N.; Ameen, F. Numerical study of transient free convective mass transfer in a Walters-B viscoelastic flow with wall suction, Commun. *Nonlinear Sci. Numer. Simul.* **2011**, *16*, 216–225. [CrossRef]
9. Rashid, M.M.; Hayat, T.; Keimanesh, M.; Yousefian, H. A study on heat transfer in a second grade fluid through a porous medium with the modified differential transform method. *Heat Transf. Asian Res.* **2013**, *42*, 31–45. [CrossRef]
10. Qasim, M.; Khan, Z.H.; Khan, W.A.; Shah, I.A. MHD boundary layer slip flow and heat transfer of ferrofluid along a stretching cylinder with prescribed heat flux. *PLoS ONE* **2014**, *9*, e83930. [CrossRef] [PubMed]
11. Gul, A.; Khan, I.; Shafie, S.; Khalid, A.; Khan, A. Heat transfer in MHD mixed convection flow of a ferrofluid along a vertical channel. *PLoS ONE* **2015**, *10*, e0141213. [CrossRef] [PubMed]
12. Ellahi, R.; Hassan, M.; Zeeshan, A. Study of natural convection MHD nanofluid by means of single and multi walled carbon nanotubes suspended in a salt water solutions. *IEEE Trans. Nanotechnol.* **2015**, *14*, 726–734. [CrossRef]
13. Ambreen, S.; Kashif, A.A.; Muhammad, A.S. Thermodynamics of magnetohydrodynamic Brinkman fluid in porous medium: Applications to thermal science. *J. Therm. Anal. Calorim.* **2018**, *45*, 50. [CrossRef]
14. Kashif, A.A.; Ilyas, K.; José, F.G.A. Thermal effects of magnetohydrodynamic micropolar fluid embedded in porous medium with Fourier sine transform technique. J. *Braz. Soc. Mech. Sci. Eng.* **2019**, *41*, 174–181. [CrossRef]
15. Ahmed, N.; Khan, U.; Mohyud-din, S.T. Influence of nonlinear thermal radiation on the viscous flow through a deformable asymmetric porous channel: A numerical study. *J. Mol. Liq.* **2017**, *225*, 167–173. [CrossRef]
16. Abro, K.A.; Souayeh, B.; Malik, K.; Atangana, A. Chaotic characteristics of thermal convection at smaller verse larger Prandtl number through fractal and fractional differential operators from nanofluid. *Int. J. Model. Simul.* **2022**. [CrossRef]
17. Souayeh, B.; Hdhiri, N.; Alam, M.-W.; Hammami, F.; Alfannakh, H. Convective Heat Transfer and Entropy Generation Around a Sphere Within Cuboidal Enclosure. *J. Thermophys. Heat Transf.* **2020**, *34*, 3. [CrossRef]
18. Abro, K.A.; Atangana, A.; Gómez-Aguilar, J.F. Ferromagnetic chaos in thermal convection of fluid through fractal–fractional differentiations. *J. Therm. Anal. Calorim.* **2021**. [CrossRef]
19. Souayeh, B.; Hammami, F.; Hdhiri, N.; Alam, M.W.; Yasin, E.; Abuzir, A. Simulation of natural convective heat transfer and entropy generation of nanoparticles around two spheres in horizontal arrangement. *Alex. Eng. J.* **2021**, *60*, 2583–2605. [CrossRef]
20. Basma, S.; Abro, K.A. Thermal characteristics of longitudinal fin with Fourier and non-Fourier heat transfer by Fourier sine transforms. *Sci. Rep.* **2021**, *11*, 20993. [CrossRef]
21. Pantokratoras, A.; Fang, T. Sakiadis flow with nonlinear Rosseland thermal radiation. *Phys. Scr.* **2013**, *87*, 015703. [CrossRef]
22. Abro, K.A.; Atangana, A. Synchronization via fractal-fractional differential operators on two-mass torsional vibration system consisting of motor and roller. *J. Comput. Nonlinear Dyn.* **2021**, *16*, 121002. [CrossRef]
23. Wen, D.; Ding, Y. Effective thermal conductivity of aqueous *Suspens.* of carbon nanotubes. *J. Thermophys. Heat Transf.* **2004**, *18*, 481–485. [CrossRef]
24. Abro, K.A.; Abdon, A. A computational technique for thermal analysis in coaxial cylinder of one-dimensional flow of fractional Oldroyd-B nanofluid. *Int. J. Ambient. Energy* **2021**. [CrossRef]
25. Awan, A.U.; Aziz, M.; Ullah, N.; Nadeem, S.; Abro, K.A. Thermal analysis of oblique stagnation point low with slippage on second-order fluid. *J. Therm. Anal. Calorim.* **2021**. [CrossRef]
26. Caputo, M.; Fabrizio, M.A. New definition of fractional derivative without singular kernel. *Prog. Fract. Diff. Appl.* **2015**, *1*, 73–85.
27. Abro, K.A.; Atangana, A. Strange Attractors and Optimal Analysis of Chaotic Systems based on Fractal-Fractional Differential Operators. *Int. J. Model. Simul.* **2021**. [CrossRef]
28. Abro, K.A.; Muhammad, N.M.; Gomez-Aguilar, J.F. Functional application of Fourier sine transform in radiating gas flow with non-singular and non-local kernel. *J. Braz. Soc. Mech. Sci. Eng.* **2019**, *41*, 400. [CrossRef]
29. Kashif, A.A. Numerical study and chaotic oscillations for aerodynamic model of wind turbine via fractal and fractional differential operators. *Numer. Methods Partial. Differ. Equ.* **2020**, 1–15. [CrossRef]
30. Abro, K.A.; Gomez-Aguilar, J.F. A comparison of heat and mass transfer on a Walter's-B fluid via Caputo-Fabrizio versus Atangana-Baleanu fractional derivatives using the Fox-H function. *Eur. Phys. J. Plus* **2019**, *134*, 101. [CrossRef]
31. Memon, I.Q.; Abro, K.A.; Solangi, M.A.; Shaikh, A.A. Functional shape effects of nanoparticles on nanofluid suspended in ethylene glycol through Mittage-Leffler approach. *Phys. Scr.* **2020**, *96*, 025005. [CrossRef]
32. Abro, K.A.; Anwar, A.M.; Muhammad, A.U. A comparative mathematical analysis of RL and RC electrical circuits via Atangana-Baleanu and Caputo-Fabrizio fractional derivatives. *Eur. Phys. J. Plus* **2018**, *133*, 113. [CrossRef]

33. Akram, S.; Ghafoor, A.; Nadeem, S. Mixed convective heat and Mass transfer on a peristaltic flow of a non-Newtonian fluid in a vertical asymmetric channel. *Heat Transf. Asian Res.* **2012**, *41*, 613–633. [CrossRef]
34. Akram, S.; Nadeem, S. Simulation of heat and mass transfer on peristaltic flow of hyperbolic tangent fluid in an asymmetric channel. *Int. J. Numer. Methods Fluids* **2012**, *70*, 1475–1493. [CrossRef]
35. Akram, S.; Athar, M.; Saeed, K.; Razia, A.; Muhammad, T. Hybridized consequence of thermal and concentration convection on peristaltic transport of magneto Powell–Eyring nanofluids in inclined asymmetric channel. *Math. Methods Appl. Sci.* **2021**. [CrossRef]
36. Akram, S.; Athar, M.; Saeed, K.; Muhammad, T.; Umair, M.Y. Partial Slip Impact on Double Diffusive Convection Flow of Magneto-Carreau Nanofluid through Inclined Peristaltic Asymmetric Channel. *Math. Probl. Eng.* **2021**, *2021*, 2475846. [CrossRef]
37. Akram, S.; Athar, M.; Saeed, K. Numerical simulation of effects of Soret and Dufour parameters on the peristaltic transport of a magneto six-constant Jeffreys nanofluid in a non-uniform channel: A bio-nanoengineering model. *Eur. Phys. J. Spec. Top.* **2021**. [CrossRef]
38. Aidaoui, L.; Lasbet, Y.; Selimefendigil, F. Effect of simultaneous application of chaotic laminar flow of nanofluid and non-uniform magnetic field on the entropy generation and energetic/exergetic efficiency. *J. Therm. Anal. Calorim.* **2021**. [CrossRef]